THE JOURNAL OF PHYSICAL CHEMISTRY C

Article

pubs.acs.org/JPCC

Interplay of Linker Functionalization and Hydrogen Adsorption in the Metal−Organic Framework MIL-101

Petra Ágota Szilágyi*

[†]Department of Imaging and Applied Physics, Curtin University, GPO Box U 1987, Perth, Western Australia 6845, Australia

Ingrid Weinrauch, Hyunchul Oh, and Michael Hirscher

Max-Planck-Institut für Metallforschung, Heisenbergstrasse 3, D-70569 Stuttgart, Germany

Jana Juan-Alcañiz, Pablo Serra-Crespo, Moreno de Respinis, Bartek Jacek Trześniewski, Freek Kapteijn, Hans Geerlings, Jorge Gascon, and Bernard Dam

Department of Chemical Engineering, Delft University of Technology, Julianalaan 136, 2628 BL Delft, The Netherlands

Anna Grzech

Civil Engineering and Geosciences, Delft University of Technology, Stevinweg 1, 2628 CN Delft, The Netherlands

Roel van de Krol

Helmholtz-Zentrum Berlin für Materialien und Energie, Institute for Solar Fuels, Hahn-Meitner-Platz 1, 14109 Berlin, Germany

Hans Geerlings

Shell Technology Centre, Grasweg 31, 1031 HW Amsterdam, The Netherlands

Supporting Information

ABSTRACT: Functionalization of metal−organic frameworks results in higher hydrogen uptakes owing to stronger hydrogen−host interactions. However, it has not been studied whether a given functional group acts on existing adsorption sites (linker or metal) or introduces new ones. In this work, the effect of two types of functional groups on MIL-101 (Cr) is analyzed. Thermal-desorption spectroscopy reveals that the −Br ligand increases the secondary building unit's hydrogen affinity, while the $-NH_2$ functional group introduces new hydrogen adsorption sites. In addition, a subsequent introduction of −Br and $-NH_2$ ligands on the linker results in the highest hydrogen-store interaction energy on the cationic nodes. The latter is attributed to a push-and-pull effect of the linkers.

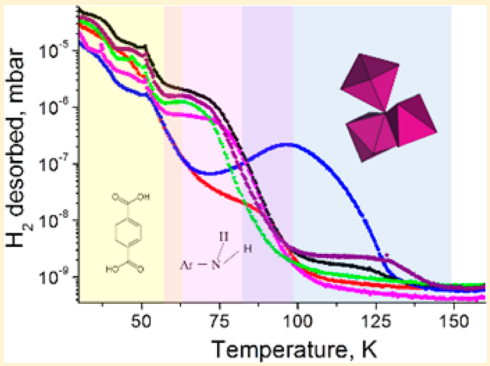

INTRODUCTION

The urgent need for strategies to reduce our fossil fuel dependence has spurred many industrialized nations to turn toward alternative sources of energy. The "hydrogen economy", in which hydrogen is used as a "green" feedstock in fuel cells to power motor vehicles, homes, and so on, has been highlighted as a potential solution to the energy problem. Challenges to be faced before this becomes a reality include the development of sustainable and fossil-free methods of hydrogen production, the safe and reversible storage and transport of hydrogen, development of affordable hydrogen fuel cells, as well as the development of efficient and reliable hydrogen sensors.[1]

Among these issues, hydrogen storage is arguably the biggest challenge. While different types of materials are being explored as hydrogen carriers, porous materials have the advantage of offering fast kinetics for hydrogen sorption as well as

Received: May 22, 2014
Revised: July 30, 2014
Published: July 31, 2014

   dx.doi.org/10.1021/jp5050628 | J. Phys. Chem. C 2014, 118, 19572−19579

reversibility over multiple cycles. Among them, metal−organic frameworks (MOFs) are considered as promising materials for nondissociative hydrogen adsorption. They are organic−inorganic hybrid materials displaying high crystallinity as well as high and regular porosity. In addition, their syntheses can be carried out under mild conditions, allowing for their rational design and facile pre- and postsynthetic modification.[2]

While some MOFs display extraordinarily high hydrogen uptake at cryogenic temperatures, as a result of the generally low enthalpy of hydrogen adsorption (ca. 2−8 kJ mol^{-1})[2−4] being considerably lower than the ideal adsorption enthalpy allowing for ambient-temperature hydrogen storage (15−25 kJ mol^{-1}),[5,6] their hydrogen capacity is practically negligible near ambient conditions, a serious drawback for application. Several ways have been identified leading to enhanced hydrogen-storage capacities in metal−organic frameworks, via two major mechanisms: (i) increase of the surface area or (ii) increase of the isosteric heat of adsorption. It has been shown through calculations and experimental results that a qualitative linear relationship exists between the H_2 storage capacities and the specific surface areas.[7,8] However, this relation is only valid at high hydrogen loading (i.e. at low temperatures and high pressures).

On the other hand, it has been shown that chemical functionalization of MOFs (i.e., the chemical modification of their building blocks) can lead to increased ambient-temperature hydrogen uptake[9] and to higher enthalpies of hydrogen adsorption. This can take place by two major mechanisms: (i) by the introduction of additional adsorption sites (on the functional groups) or (ii) by the secondary effect of the functionalities on the frameworks' polarity (cf., by increasing the secondary building unit's hydrogen affinity). This latter phenomenon can be aided by the fact that adsorption of hydrogen on porous materials is driven by the van der Waals interaction or by the Debye force (between a permanent dipole and an induced dipole in the hydrogen molecule). Addition of polar functional groups in the linkers strengthens the Debye force, regardless of whether the hydrogen molecule interacts with the positive or the negative part of the dipole. Since MOF linkers are aromatic organics, the addition of functional groups will not only yield stronger dipoles on the functional group but it will also polarize the whole linker and the linker−secondary building unit (SBU, or metal node) bond. Such phenomenon has been shown to remarkably affect catalytic activity of the extremely stable UiO-66, owing to the electronic modulation of the active site by functionalization.[10] Similarly, the impact of the polarization of the linker-secondary building unit through linker functionalization on the photocatalytic activity of isoreticular MOFs has also been recently reported.[11]

Despite the obvious interest and research efforts, the mechanism of how linker functionalization affects the hydrogen−framework interaction has never been studied directly. In particular, there is a desperate lack of information whether a given functional group acts on existing adsorption sites (linker or metal) or introduces new ones.

In this work, we analyze the effect of two types of functional groups on MIL-101(Cr) ($Cr_3FO[BDC]_3$, BDC = 1,4-benzenedicarboxylate). MIL-101(Cr) has been chosen as a starting material, owing to its high surface area, its high hydrogen uptake at 77 K, and outstanding chemical stability.[12] Although MIL-101 has been suggested as not a possible starting material for solvent-assisted linker exchange (SALE),[13] we have recently shown that postsynthetic cation exchange is possible in the same material,[14] suggesting that postsynthetic linker exchange may also be possible. 2Br-BDC and 2-NH_2-BDC (for molecular structures, see Figure S1 of the Supporting Information) were chosen as substitute linkers for their highly electronegative functional groups that may allow for different types of interactions with the adsorbent hydrogen molecules; while the −Br functionality is highly polarizable and can thus partake in strong van der Waals interactions, the $-NH_2$ functionality may allow for more specific interactions through its lone electron pair or via dihydrogen bonding. In addition, de Vos and colleagues showed that the −Br and $-NH_2$ functional groups change the Lewis acidity of the metal corner in the opposite way: whereas −Br ligands increase Lewis acidity, $-NH_2$ groups were found to decrease it due to electronic effects on the terephthalate linker.[10] Although of all functional groups they studied the $-NO_2$ and $-NH_2$ groups showed the greatest difference in their impact on the metal corner, we opted for the Br functionality as its higher electron density yields larger differences upon characterization with X-ray-based techniques. In addition, NH_2-MIL-101(Cr) cannot be prepared by direct synthetic methods without seriously compromising its crystallinity[15] and is therefore obtained by the reduction of NO_2-MIL-101(Cr) (see Materials and Methods). This results in some unconverted $-NO_2$ remaining in the framework, which would bias the distinction between the different effects. Furthermore, Yaghi and co-workers have recently shown that some MOF-5 analogs, synthesized from a mixture of linkers (the so-called multivariate, MTV, and MOFs) display enhanced gas uptake when compared with the analogs containing a single type of linkers.[16] Although, the origin of the phenomenon was not discussed, it is possible that the electronic modulation of the metal sites by a partial linker exchange may play a key role in this phenomenon. Therefore, the effect of partial functionalization of MIL-101(Cr) with 2-Br-BDC and 2-NH_2-BDC on the electronic modulation and on the types of hydrogen adsorption sites is also discussed.

MATERIALS AND METHODS

Synthetic Methods. MIL-101(Cr) and Br-MIL-101(Cr) were prepared by direct hydrothermal synthesis, mixing chromium(III) nitrate $Cr(NO_3)_3{\cdot}9H_2O$, hydrofluoric acid with 1,4-benzenedicarboxylic acid, and by 2-bromo-1,4-benzenedicarboxylic acid, respectively, according to Férey's method.[17] Synthesis of NH_2-MIL-101(Cr) was carried out by the chemical reduction of NO_2-MIL-101(Cr). First, NO_2-MIL-101(Cr) was synthesized similarly to MIL-101(Cr), by replacing H_2BDC by 2-nitro-1,4-benzenedicarboxylic acid. Subsequently, NO_2-MIL-101(Cr) was reduced to NH_2-MIL-101(Cr) by chemical reduction using $SnCl_2$, according to Stock and co-workers' method,[18] with the only difference being that slightly longer reaction time (16 h) was allowed.

Linker Exchange. Linker exchange was carried out as follows: 150 mg MIL-101(Cr) was refluxed for 3 h with 30 mg 2-bromo-1,4-benzenedicarboxylic acid or 25 mg 2-amino-1,4-benzenedicarboxylic acid in 150 cm^3 deionized water at 100 °C. In addition, 150 mg previously postsynthetically linker exchanged, Br-BDC-containing, MIL-101(Cr) (**BrPSM**) was refluxed for 3 h with a 25 mg 2-amino-1,4-benzenedicarboxylic acid in 150 cm^3 deionized water at 100 °C.

Activation of Samples. All MOF samples were activated for 6 h in vacuo at 160 °C following water-to-tetrahydrofuran solvent exchange.

dx.doi.org/10.1021/jp5050628 | J. Phys. Chem. C 2014, 118, 19572−19579

Diffuse Reflectance Infra-Red Fourier Transform (DRIFTS). Spectra were recorded on a Nicolet model 8700 spectrometer, equipped with a high-temperature cell, and a DTGS-TEC detector. The spectra were acquired with 256 scans at 4 cm^{-1} resolution from 4000 to 500 cm^{-1} using potassium bromide (KBr) to perform background experiments. The samples were pretreated at 453 K for 1 h in a helium flow of 20 cm^3 min^{-1}.

UV−vis Diffuse Reflectance Spectroscopy. Spectra were measured with a Perkin−Elmer Lambda 900 spectrophotometer equipped with an integrating sphere ("'Labsphere'") in the 200−800 nm range. The Kubelka−Munk function was used to convert reflectance measurements into equivalent absorption spectra using the reflectance of $BaSO_4$ as a reference.

Determination of the Extent of Linker Substitution. The extent of postsynthetic linker exchange was determined by area integral of (i) the UV-vis spectra: MIL-101(Cr) spectrum was used as background subtraction, and the curve was integrated over a maximum at 380 nm, between 307 and 475 nm, as well as of that of (ii) the DRIFT spectra: a linear baseline was used as background for the integration of symmetric and asymmetric $\nu(-NH_2)$ between 3317 and 3545 cm^{-1}, with maximum peaks around 3370 and 3520 cm^{-1}, respectively. In the case of the Br-BDC-containing samples, the sum of the normalized and baseline-corrected ortho- and meta-substituted Ar−Br stretch combination modes (at 1042 and 1072 cm^{-1}, respectively) was used to determine the extent of the linker exchange.

Nuclear Magnetic Resonance Spectroscopy. Because of the highly paramagnetic Cr^{3+} ions, a customized digestion method was applied for the SALE-modified samples: the samples were digested in an aqueous H_2O_2 solution, which also allowed for the oxidation of the Cr^{3+} ions. The solvent was subsequently evaporated and the organic part of the remaining powder was dissolved in deuterated DMF. Proton NMR spectra were recorded on the digested samples using a Bruker Avance-400 spectrometer. We would like to note that due to the complexity of the digestion method (hindered by the necessity of controlled oxidation states, linker solubility, and signal multiplicity issues) and the consequent uncertainty of the preservation of linker ratios, we only used the NMR spectra to demonstrate the presence of various linkers.

Scanning Electron Microscopy. Shape, size, and morphology of all samples were investigated by SEM (JSM-7500F) using an electron beam energy of 5 keV.

Synchrotron X-ray Powder Diffraction and Analysis. Diffraction data were collected on the ID31 beamline at the European Synchrotron Radiation Facility using a monochromatic X-ray beam of λ = 0.4305 Å. Each sample was activated prior to data collection and subsequently loaded into capillaries in an Ar glovebox. The capillary was being spun throughout the SXRPD data collection, which was detected using a series of 9 multianalyzing Si (1 1 1) crystal detectors.[19] Cell parameters of the samples were determined in the $Fd\bar{3}m$ space group, as found by Férey and colleagues for the pristine MIL-101(Cr),[17] using the LeBail refinement mode as implemented in the GSAS analytical software package.[20] Due to the low-angle asymmetry, lattice parameters and Gaussian line shapes were determined from the higher angle region (1.5−3 deg) and subsequent peak-shape fitting was carried out on the whole pattern, leaving the lattice parameters and Gaussian line terms unaltered. Powder patterns of Br-MIL-101(Cr) and NH_2-MIL-101(Cr) were simulated as follows: the crystallographic information file of pristine MIL-101(Cr)[17] was loaded in Wincrystals 2000[21] and missing hydrogen atoms were placed on the linkers' aromatic rings and a new crystallographic information file was generated thereof. The hydrogen atoms on the aromatic linkers were then exchanged to Br and N, respectively, their multiplicity decreased to 1/4, and the final crystallographic information files were thus generated, which were then used to simulate their powder pattern at λ = 0.4305 Å.

Determination of the Brunauer−Emmett−Teller (BET) Surface Area. N_2 adsorption of the activated samples was carried out using an Autosorb 6B-type nitrogen-adsorption instrument at 77 K. The isotherms obtained were then fitted using the BET function, as implemented in the instrument's software package.

Hydrogen Adsorption. Hydrogen adsorption and desorption isotherms were recorded at 298 and 77 K, in a Sievert's apparatus (HyEnergy, PCTPro-2000) up to ca. 30 bar hydrogen pressure. Due to their sensitivity toward moisture, the activated samples were loaded into the microdoser in a glovebox, under Ar atmosphere.

High-resolution, low-temperature hydrogen-sorption isotherms of MOF samples at 19.5 K were measured with laboratory-designed volumetric adsorption equipment with a temperature-controlled cryostat. Around 23 mg of MOF samples were activated under ultrahigh vacuum at 150 °C overnight, prior to each measurement. For the laboratory-designed cryostat, the temperature control was calibrated by measuring the liquefaction pressure for hydrogen and nitrogen in the empty sample chamber at various temperatures.

Thermal Desorption Spectroscopy (TDS). TDS spectra of H_2 and D_2 were acquired using the setup described in ref 22 as follows: prior to the measurement, a 2−4 mg sample was heated at 470 K in high vacuum (below 10^{-5} mbar) for approximately 3 h to remove moisture and adsorbed gases. Then the sample was slowly cooled down to approximately 20 K and was loaded with 10 mbar of hydrogen or deuterium. After the addition of the gas, the sample was kept under pressure at 20 K for 5 min. Subsequently, the reactor was evacuated for several minutes (final pressure was below 10^{-7} mbar) to remove the nonadsorbed hydrogen (or deuterium) molecules. Owing to the low temperature of the sample, adsorbed H_2 and D_2 stick to the surface of the adsorbent even under vacuum, while the free molecules can be easily pumped off. Then the temperature program was started with a constant heating rate of 0.1 K s^{-1}, and the signal of desorbed hydrogen, deuterium, and HD molecules was recorded with the mass spectrometer. In addition, the masses 1 and 18 of atomic hydrogen and water, respectively, were measured. Desorption spectra were recorded up to 160 K. Several spectra were acquired up to 300 K, and as no hydrogen desorption occurred above 160 K, the rest of the spectra were only acquired up to 160 K.

Integration of the desorption peaks was performed by the subtraction of baseline defined from the high-temperature range (above 150 K) of the spectra, subsequently, Gaussian peak shapes were fitted whose area is proportional to the number of gas molecules desorbed and can be quantified after calibration.

Thermogravimetrical Analysis (TGA). Thermal analysis of the materials (Figure S9 of the Supporting Information) was carried out using a system provided by Mettler Toledo, model TGA/SDTA851e. First the samples were treated under air flow

dx.doi.org/10.1021/jp5050628 | J. Phys. Chem. C 2014, 118, 19572−19579

at 323 K to eliminate moisture for 1 h and then analyzed under an air flow of 60 cm^3 min^{-1} at a temperature rate of 5 K min^{-1}.

RESULTS AND DISCUSSION

In order to investigate the mechanism of the effect of linker functionalization on the hydrogen−framework interaction, MIL-101(Cr)[17] and NH_2-MIL-101(Cr)[18] have been synthesized according to the literature, Br-MIL-101(Cr) has been synthesized analogously to MIL-101(Cr). In addition, solvent-assisted linker-exchange was applied to obtain postsynthetically modified (PSM), partially linker-exchanged **BrPSM** [2-Br-BDC-substituted MIL-101(Cr)], **NH_2PSM** [2-NH_2−BDC-substituted MIL-101(Cr)], and **BrNH_2PSM** [2-NH_2−BDC and 2-Br-BDC-substituted MIL-101(Cr)]. We have identified a successful linker exchange, as demonstrated by UV-vis (Figure S2 of the Supporting Information), DRIFT (Figure S3 of the Supporting Information), and ^{1}H NMR spectroscopy (see Experimental and Figure S1 of the Supporting Information). From these data, the extent of the linker exchange could be determined, which amounts to ca. 20% of all linkers (Table S1 of the Supporting Information).

First, the samples' hydrogen-storage properties were probed by equilibrium adsorption experiments at 77 and 298 K. Figure 1 shows the adsorption isotherms of the MTV and pristine

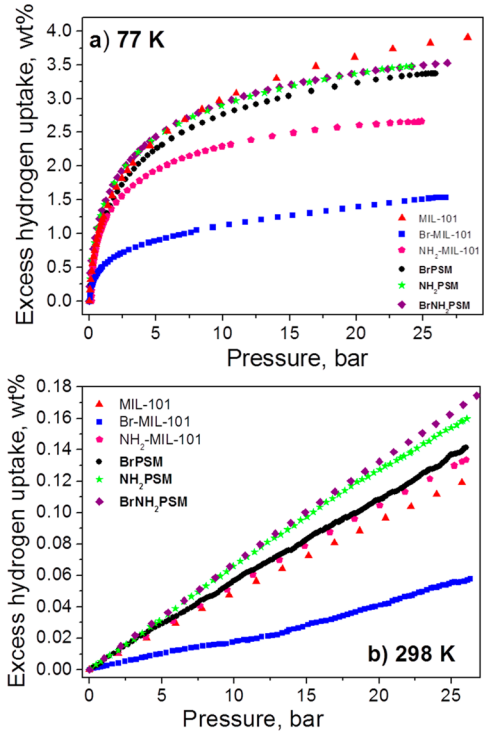

Figure 1. H_2-sorption isotherms of MIL-101(Cr), Br-MIL-101(Cr), NH_2-MIL-101(Cr), and samples **BrPSM**, **NH_2PSM**, and **BrNH_2PSM** at (a) 77 K and (b) 298 K.

(containing only one kind of linker) MOFs. At 77 K, the pristine MIL-101(Cr) shows the highest hydrogen uptake, in good agreement with the N_2 physisorption measurements at the same temperature (Table S2 of the Supporting Information). In other words, the saturation hydrogen uptake (the concentration beyond which hydrogen uptake does not increase further with increasing hydrogen pressure) was found to be governed by the available surface area (MIL-101, 2136 m^2 g^{-1}; Br-MIL-101, 840.6 m^2 g^{-1}; NH_2-MIL-101, 2001 m^2 g^{-1}; **BrPSM**, 1940 m^2 g^{-1}; **NH_2PSM**, 2059 m^2 g^{-1}; and **BrNH_2PSM**, 1839 m^2 g^{-1}), as displayed in the low-temperature hydrogen isotherm (Figure 1a). In contrast, at ambient temperature and at much lower hydrogen loadings, the hydrogen uptake of samples **BrPSM**, **NH_2PSM**, and **BrNH_2PSM** is 20−40% higher than that of MIL-101(Cr). In addition, NH_2-MIL-101(Cr) also showed relatively high hydrogen-adsorption capacity at room temperature, while Br-MIL-101(Cr) again shows the lowest hydrogen uptake. In addition, hydrogen uptake per formula unit was observed to increase compared to that of MIL-101(Cr) (0.393 mol H_2) by 50% for **BrNH_2PSM** (0.573 mol H_2) under 25 bar hydrogen pressure at 298 K. **BrPSM** (0.471 mol H_2), **NH_2PSM** (0.524 mol H_2), and NH_2-MIL-101(Cr) (0.446 mol H_2) also showed increased hydrogen uptake per formula unit, while Br-MIL-101(Cr) (0.207 mol H_2) showed poorer performance at 298 K.

If the impact of linkers on the amount and nature of hydrogen adsorption sites is to be investigated, a number of other effects that may also result in increased hydrogen uptake need to be safely excluded. Trivial reasons such as a phase transition can be dismissed on the basis of our powder X-ray diffraction results (Figure S4 of the Supporting Information), this may be relevant as MIL-101(Cr) is known to be the thermodynamically disfavored Cr(BDC) polymorph (as opposed to MIL-53).[23]

Powder X-ray diffraction data (PXRD) were collected on all samples, and it was possible to index all patterns in the $Fd\bar{3}m$ space group (Table S3 of the Supporting Information), which confirms that the hydrogen-uptake enhancement upon SALE is not due to structural changes. It has been shown that the formation of core−shell particles may be indicated as two phases in the diffractogram in case the particles are large enough.[24] On the other hand, when the shell of core−shells crystallites are too thin to diffract individually, broadening of the diffraction peaks of the core would be observed, since the same batch of MIL-101(Cr) was used for the solvent-assisted linker exchange and powder X-ray diffraction data collection. The reason for such a line broadening would be the following: while the crystallite size of the starting and postsynthetically modified samples remains the same (for SEM images see Figure S6 of the Supporting Information), the particles would be built up of two substructures (core and shell), with different lattice parameters [as determined from the powder pattern of the pure MIL-101(Cr), Br-MIL-101(Cr), and NH_2-MIL-101(Cr)]. The particle sizes observed in the PXRD pattern would thus appear to be smaller, which, in turn, would result in line broadening. We have observed that the pattern in each diffractogram displays one phase only. In addition, the peak-shape analysis of the diffraction pattern shows that the obtained crystallites are comparable in size with the initial ones. It can thus be safely concluded that the postsynthetic linker-exchange took place randomly throughout the particles' pore space.

In addition, pore narrowing in the case of NH_2-MIL-101(Cr) can also play some role, which might be a consequence of its indirect preparation.[18,25] The reaction pathway for the indirect preparation route does not allow for the complete removal of the reactant from the pores to a small extent, which in turn may modify the material's hydrogen uptake.[26] In contrast, further analysis of the diffraction data reveals that pore narrowing can be excluded as the reason for the increase of the hydrogen uptake in the postsynthetically modified samples. The (0 2 2): (1 1 3) diffraction peak ratio has been highlighted as a sensitive

dx.doi.org/10.1021/jp5050628 | J. Phys. Chem. C 2014, 118, 19572−19579

Table 1. Comparison of Hydrogen Adsorption Enthalpies for MIL-101(Cr), Br-MIL-101(Cr), NH_2-MIL-101(Cr), and Samples BrPSM, NH_2PSM, and $BrNH_2$PSM at 0.2 wt % Loading

material	MIL-101[a]	Br-MIL-101	NH_2-MIL-101	**BrPSM**	**NH_2PSM**	**$BrNH_2$PSM**
ΔH_{ads}, kJ mol^{-1}	4.23(1)	4.10(2)	4.31(2)	4.27(4)	4.28(4)	4.32(2)

[a]Somewhat lower but still in agreement with the literature data.[29]

measure of pore filling.[27] On the other hand, our simulations show that linker substitution does not have a large impact on the above diffraction peak ratio and indeed we have not observed any substantial change upon postsynthetic linker exchange (Figure S5 of the Supporting Information), confirming that the increase of the hydrogen uptake is due to linker substitution and not to pore narrowing.

In the case of the framework's electronic modulation by linker exchange, the Debye forces of the hydrogen−framework interaction should change significantly, in particular on the modulated sites of the framework such as the metal nodes or the linker functionalities. As these latter ones may also act as added adsorption sites, the host−hydrogen interactions would be further modified. Attention needs to be drawn to the differences in the enthalpies of adsorption of hydrogen on the various sites of the frameworks: for example, it has been shown that hydrogen has a stronger interaction with the metal unit than with the aromatic ring.[28] In order to probe the effect of linker-exchange on the strength of Debye interactions between the framework and the hydrogen molecules, the enthalpy of hydrogen adsorption has been determined at hydrogen loading of 0.2 wt % (Table 1), close to the maximum uptake at ambient temperature. Our results show a very slight increase of the adsorption enthalpy at relatively low (0.2 wt %) hydrogen loading, when compared with the pristine MIL-101(Cr).

It can thus be concluded that linker functionalization increases the ambient temperature hydrogen uptake of MIL-101(Cr), although the gravimetric hydrogen uptake in this regime for the fully functionalized Br-MIL-101(Cr) was not enhanced due to the large mass of the framework. The increased hydrogen uptake can be attributed to a stronger hydrogen−host interaction, as reflected by the enthalpies of adsorption measured. This is in line with previous observations;[5,6] however, it does not reveal the underlying physical phenomena. As an example, NH_2-MIL-101(Cr) and **BrPSM** show similar adsorption isotherms at both, 77 and 298 K; in addition, the enthalpies of hydrogen adsorption on them are also a fair match, despite having different functional groups and a different extent of linker functionalization.

In order to reveal the effect of electronic modulation by linker substitution and of those of the linker functional groups as adsorption sites, the hydrogen−framework interactions need to be analyzed in detail. Thermal desorption spectroscopy has been highlighted as an unrivalled tool to get insight into the strength of hydrogen−host interactions.[22,29,30] Desorption of hydrogen as a function of temperature from all samples was therefore monitored.

Note that the sharp peaks at ca. 25 and 50 K are artifacts; they are a consequence of the change of PID parameters.

In the TDS spectra, various desorption ranges corresponding to different adsorption sites are clearly discernible and can be divided into three regions (Figure 2). The lowest temperature region (up to ca. 40 K) can be described as the convolution of the desorption signals from the weakest adsorption sites, aromatic rings, for instance, and the boiling of the liquid hydrogen trapped in the pores.

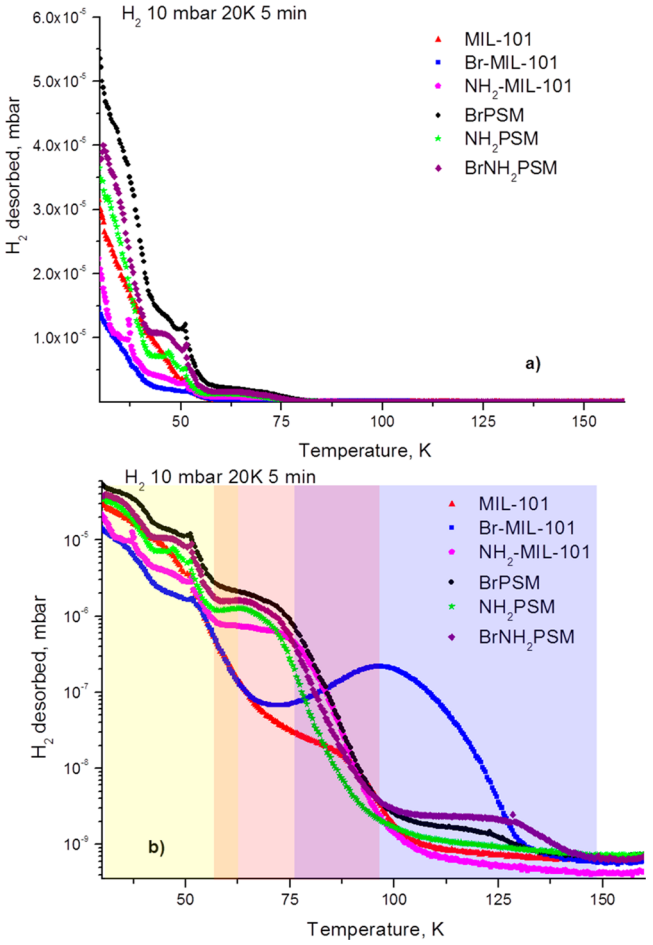

Figure 2. TDS spectra of hydrogen from various MOFs shown on (a) linear and (b) semilogarithmic scales, showing the three different desorption regions: desorption from the pores and linkers (yellow), desorption from the functional groups of the linkers (pink), and desorption from the SBU (blue). Note that the range of the three different regions varies somewhat for different linkers, thus the intermediate regions (orange and purple).

Between ca. 40 and 70 K desorption off the linkers is displayed in the spectra (Figure 2a). While MIL-101(Cr) and Br-MIL-101(Cr) yield only one desorption peak in this region, the appearance of an additional peak centered between 60 and 70 K can be observed for the case of NH_2-MIL-101(Cr) (Figure 2b). In addition, this last peak is also present in the spectra of all the amino functional-group-containing samples (**NH_2PSM** and **$BrNH_2$PSM**). As this is the only additional peak in the TDS spectrum of NH_2-MIL-101(Cr), the hypothesis of the increased hydrogen uptake being the consequence of pore narrowing by the remaining $SnCl_2$ can be excluded. The reason for this is that this peak is identical to those found on the postsynthetically functionalized $-NH_2$-containing **NH_2PSM** and **$BrNH_2$PSM**, which do not contain $SnCl_2$ in their pores. This suggests that the introduction of

dx.doi.org/10.1021/jp5050628 | J. Phys. Chem. C 2014, 118, 19572−19579

$-NH_2$ groups in the MOF's framework introduces new adsorption sites.

On the other hand, fully functionalized Br-MIL-101(Cr) apparently does not have more (or different) hydrogen adsorption sites than the pristine MIL-101(Cr). Partially linker-exchanged **BrPSM**, however, displays similar behavior to the samples containing amino functionalities. One possible explanation for this phenomenon is that the organic functional group would polarize the whole aromatic linker. If the linkers are substituted in a symmetrical and ordered fashion, some of the polarization would be lost, as the influence of two functionalized linkers may counterbalance each other. Conversely, random linker substitution results in stronger dipole interactions and, therefore, a stronger interaction between H_2 and its adsorption site.

The highest temperature region of the TDS spectra (i.e., above 80 K) corresponds to hydrogen desorption off the inorganic building unit (Figure 1a). A striking feature of the spectra in this region is that whenever −Br ligands are present, the desorption temperature is shifted to higher temperature values. This reveals that the addition of Br functionalities will polarize the linker−secondary building unit bond; this observation has also been confirmed by our low-temperature hydrogen adsorption data (Figure S7 of the Supporting Information).

The fact that no such effect has been observed for amino functionalities is in line with the observations of de Vos et al. who found that −Br ligands increase Lewis acidity while $-NH_2$ groups were found to decrease it.[7] It can be thus assumed in a first instance that, in order to obtain stronger hydrogen−SBU interactions, stronger Lewis acids need to be applied on the cationic nodes. On the other hand, the highest hydrogen desorption temperature has been observed in the case of **$BrNH_2$PSM**. This phenomenon can be explained by the two opposite effects of the $-NH_2$ and −Br functional groups, resulting in a push-and-pull force, which in turn further increases the hydrogen affinity of the site.

Desorption of deuterium shows very similar trends to that of hydrogen, confirming that the observed phenomena are only related to desorption of hydrogen from the frameworks (Figure S8 of the Supporting Information).

Upon integrating the peaks in the TDS spectra, a qualitative analysis of the desorption of hydrogen from the MOFs can be carried out and the results are summarized in Table 2.

The three regions mentioned above (highlighted in Figure 2b) can now be quantified as (i) convolution of hydrogen liquid boil off from the pores and desorption from the lowest enthalpy adsorption sites takes place in the 30−40 K region; (ii) hydrogen desorbs from the functional groups in the 40−70 K region, and (iii) from the secondary building unit in the 70−120 K region. Overlap of the distinct region is due to different temperatures of hydrogen desorption in the different MOFs.

The opposite effect of the −Br and $-NH_2$ groups on the Lewis acidity of the secondary building can also be observed upon close inspection of the data in Figure 2. The desorption peak of hydrogen from the SBU of pristine MIL-101(Cr) is centered at about 87 K, which was increased to 96 K on a total Br-functionalization and did not substantially change for NH_2-MIL-101(Cr), resulting in its desorption peak practically overlapping with that of the functional groups.

As the materials only adsorb up to ca. 0.2 wt % at 298 K under ca. 30 bar hydrogen pressure, the TDS spectra explain why NH_2-MIL-101(Cr), **BrPSM**, **NH_2PSM**, and **$BrNH_2$PSM** have the highest uptake under these conditions: at this uptake range (up to 0.2 wt %), the adsorption is governed by the functional groups and their random distribution. As Br-MIL-101(Cr) and MIL-101(Cr) have no functional groups that could adsorb in this region, their hydrogen uptake is consequently lower. Although Br-MIL-101(Cr) displays an increased hydrogen uptake on the SBUs, this phenomenon is of such a low extent in terms of the number of hydrogen molecules adsorbed that it practically has no effect in the ambient-temperature hydrogen isotherm. In fact, ambient-temperature isotherms and the TDS maxima at higher temperatures show ca. 0.1 wt %, which corresponds to a lower than 10% occupancy of the available adsorption sites. In addition, the slight increase of the enthalpies of hydrogen adsorption on the postsynthetically modified samples can also be rationalized as the adsorption in the up to 0.2 wt % range is governed by the linkers, including the functional groups. While at this loading the increase of the adsorption enthalpies is below 2.5%, it is anticipated that at zero coverage the difference is substantially larger, as reflected by the ca. 40 K higher hydrogen-desorption temperature from the secondary building unit of **$BrNH_2$PSM** than that of the pristine MIL-101(Cr) (Figure 2b), at the applied 0.1 K s^{-1} heating rate.

While both functionalities improved hydrogen−framework interactions (the −Br ligand increases the SBU's hydrogen affinity, while the $-NH_2$ functional group introduces new hydrogen adsorption sites), the introduction of amino groups can be a more viable option for hydrogen-storage applications since the increased hydrogen uptake due to the SBUs' higher

Table 2. Analysis of TDS Spectra[a]

MOF	desorption temperature (center, K)	wt %	desorption site−region	in 298 K isotherm
MIL-101(Cr)	87	10^{-4}	SBU	yes
	38	0.6	linker +	partly
	30	1.1	H_2 boil off	no
Br-MIL-101(Cr)	96	0.02	SBU	yes
	46	0.1	linker +	yes
	32	0.4	H_2 boil off	partly
NH_2-MIL-101(Cr)	Up to 75	10^{-4}	SBU	yes
	64	0.1	functionality	yes
	43	0.2	linker +	partly
	31	0.4	H_2 boil off	no
BrPSM	114	10^{-4}	SBU	yes
	64	0.1	functionality	yes
	45	0.6	linker +	partly
	34	1.7	H_2 boil off	no
NH_2PSM	up to 87	7×10^{-5}	SBU	yes
	62	0.1	functionality	yes
	46	0.5	linker +	partly
	33	1.2	H_2 boil off	no
$BrNH_2$PSM	118	1.5×10^{-4}	SBU	yes
	62	0.1	functionality	yes
	46	0.5	linker +	partly
	31	1.2	H_2 boil off	no

[a]This analysis also highlights that at a 0.2 wt % loading, hydrogen desorbs at higher temperatures (owing to stronger hydrogen−host interactions) in the case of the three postsynthetically modified samples and NH_2-MIL-101(Cr) than in the cases of the pristine MIL-101(Cr) and Br-MIL-101(Cr), in good agreement with the adsorption enthalpies determined.

dx.doi.org/10.1021/jp5050628 | J. Phys. Chem. C 2014, 118, 19572−19579

hydrogen affinity has only a minor effect (an additional 0.02 wt %, although at relatively high temperatures partial linker-exchanged samples have proven to be the best option as they benefit from both effects, in particular for the MOF containing both types of functional groups, which shows the strongest hydrogen−SBU interaction.

CONCLUSIONS

In the present work, the effect of linker substitution on the electronic modulation of the MIL-101(Cr) metal−organic framework has been studied. Particular emphasis was given to the hydrogen−host interactions as a function of the electronic properties of the substituting linkers as well as the extent of linker substitution (total or partial). In order to achieve partial linker exchange, solvent-assisted linker exchange in MIL-101(Cr) was successfully employed and it was found that it results in increased ambient-temperature hydrogen uptake due to stronger hydrogen−host interactions, as reflected in the enthalpies of hydrogen adsorption. Our results suggest that −Br functionalities act mainly on the metal site and do not form an independent adsorption site (unless only partially introduced into the framework). In contrast, $-NH_2$ functionalities do not improve the metal-site−hydrogen interaction substantially, but they do form additional adsorption sites. Partial linker exchange did not yield a lot of difference in comparison with the total functionalization when only $-NH_2$ groups were introduced in MIL-101(Cr), apart from the obvious difference in the molar mass. Subsequent introduction of −Br and $-NH_2$ ligands resulted in the highest hydrogen-store interaction energy on the cationic nodes. The latter is attributed to the opposite electronic modulating effect, push-and-pull, of the distinct linkers. While these observations highlight the importance of functional groups when addressing hydrogen storage in metal−organic frameworks, the resultant ambient-temperature hydrogen-uptake increase is too small for applications. Furthermore, the knowledge generated on the adsorption mechanism of hydrogen on functionalized MOFs may be beneficial for gas separation and catalytic applications.

ASSOCIATED CONTENT

Supporting Information

NMR spectra, UV−vis spectra, DRIFT spectra with assignments, linker compositions calculated, BET surface areas, SPXRD patterns with Le Bail fits, lattice parameters determined, SEM images, low-temperature high-resolution hydrogen adsorption isotherms, D_2 desorption spectra, and TGA curves. This material is available free of charge via the Internet at http://pubs.acs.org.

AUTHOR INFORMATION

Corresponding Author

*E-mail: Petra.Szilagyi@curtin.edu.au.

Author Contributions

The manuscript was written through contributions of all authors. All authors have given approval to the final version of the manuscript.

Notes

The authors declare no competing financial interest.

ACKNOWLEDGMENTS

The authors thank the Agenstchap.nl (Energy Innovation Funding Agency) for funding (Grant EOSLT07052) and the European Synchrotron Radiation Facility for provision of beamtime. Particular thanks are due to Ruben Abellon, Frans Oostrum, and Willy Rook for experimental support.

ABBREVIATIONS

MOF: metal−organic framework; SBU: secondary building unit; BDC: 1,4-benzenedicarboxylic acid; MTV: multivariate; SALE: solvent-assisted linker exchange; PSM: postsynthetic modification; UV−vis: UV−visible; DRIFT: diffuse reflectance infrared; NMR: nuclear magnetic resonance; PXRD: powder X-ray diffraction; SPXRD: synchrotron powder X-ray diffraction; SEM: scanning electron microscopy; TDS: thermal desorption spectroscopy; PID: photoionization detector; BET: Brunauer−Emmett−Teller

REFERENCES

(1) Tollefson, J. Hydrogen Vehicles: Fuel of the Future? *Nature* **2010**, 1262−1264.

(2) Sculley, J.; Yuan, D.; Zhou, H.-C. The Current Status of Hydrogen Storage in Metal−Organic Frameworks—Updated. *Energy Environ. Sci.* **2011**, *4*, 2721−2735.

(3) Murray, L. J.; Dincă, M.; Long, J. R. Hydrogen Storage in Metal−Organic Frameworks. *Chem. Soc. Rev.* **2009**, *38*, 1294−1314.

(4) Zhao, D.; Yuan, D.; Zhou, H. C. The Current Status of Hydrogen Storage in Metal−Organic Frameworks. *Energy Environ. Sci.* **2008**, *1*, 222−235.

(5) Bhatia, S. K.; Myers, A. L. Optimum Conditions for Adsorptive Storage. *Langmuir* **2006**, *22*, 1688−1700.

(6) Bae, Y.-S.; Snurr, R. Q. Optimal Isosteric Heat of Adsorption for Hydrogen Storage and Delivery Using Metal−Organic Frameworks. *Microporous Mesoporous Mater.* **2010**, *132*, 300−303.

(7) Wong-Foy, A. G.; Matzger, A. J.; Yaghi, O. M. Exceptional H_2 Saturation Uptake in Microporous Metal−Organic Frameworks. *J. Am. Chem. Soc.* **2006**, *128*, 3494−3495.

(8) Panella, B.; Hirscher, M.; Pütter, H.; Müller, U. Hydrogen Adsorption in Metal−Organic Frameworks: Cu-MOFs and Zn-MOFs Compared. *Adv. Funct. Mater.* **2006**, *16*, 520−524.

(9) Rowsell, J. L.; Yaghi, O. M. Effects of Functionalization, Catenation, and Variation of the Metal Oxide and Organic Linking Units on the Low-Pressure Hydrogen Adsorption Properties of Metal−Organic Frameworks. *J. Am. Chem. Soc.* **2006**, *128*, 1304−1315.

(10) Vermoortele, F.; Vandichel, M.; van de Voorde, B.; Ameloot, R.; Waroquier, M.; van Speybroeck, V.; de Vos, D. E. Electronic Effects of Linker Substitution on Lewis Acid Catalysis with Metal−Organic Frameworks. *Angew. Chem., Int. Ed.* **2012**, *51*, 4887−4890.

(11) Gascon, J.; Hernández-Alonso, M. D.; Almeida, A. R.; van Klink, G. P. M.; Kapteijn, F.; Mul, G. Isoreticular MOFs as Efficient Photocatalysts with Tunable Band Gap: An Operando FTIR Study of the Photoinduced Oxidation of Propylene. *ChemSusChem* **2008**, *1*, 981−983.

(12) Latroche, M.; Surblé, S.; Serre, C.; Mellot-Draznieks, C.; Llewellyn, P. L.; Lee, J.-H.; Chang, J.-S.; Jhung, S. H.; Férey, G. Hydrogen Storage in the Giant-Pore Metal−Organic Frameworks MIL-100 and MIL-101. *Angew. Chem., Int. Ed.* **2006**, *45*, 8227−8231.

(13) Kim, M.; Cahill, J. F.; Fei, H.; Prather, K. A.; Cohen. Postsynthetic Ligand and Cation Exchange in Robust Metal−Organic Frameworks. S. M. *J. Am. Chem. Soc.* **2012**, *134*, 18082−18088.

(14) Szilágyi, P. Á.; Serra-Crespo, P.; Dugulan, I.; Gascon, J.; Geerlings, H.; Dam, B. Post-Synthetic Cation Exchange in the Robust Metal−Organic Framework MIL-101(Cr). *CrystEngComm* **2013**, *15*, 10175−10178.

(15) Jiang, D.; Keenan, L. L.; Burrows, A. D.; Edler, K. J. Synthesis and Post-Synthetic Modification of MIL-101(Cr)-NH_2 via a Tandem Diazotisation Process. *Chem. Commun.* **2012**, *48*, 12053−12055.

(16) Deng, H.; Doonan, C. J.; Furukawa, H.; Ferreira, R. B.; Towne, J.; Knobler, C. B.; Wang, B.; Yaghi, O. M. Multiple Functional Groups

of Varying Ratios in Metal-Organic Frameworks. *Science* **2010**, *327*, 846−850.
(17) Férey, G.; Mellot-Draznieks, C.; Serre, C.; Millange, F.; Dutour, J.; Surblé, S.; Margiolaki, I. A Chromium Terephthalate-Based Solid with Unusually Large Pore Volumes and Surface Area. *Science* **2005**, *309*, 2040−2042.
(18) Bernt, S.; Guillerm, V.; Serre, C.; Stock, N. Direct Covalent Post-Synthetic Chemical Modification of Cr-MIL-101 Using Nitrating Acid. *Chem. Commun.* **2011**, *47*, 2838−2840.
(19) Hodeau, J.-L.; Bordet, P.; Anne, M.; Prat, A.; Fitch, A. N.; Dooryhee, E.; Vaughan, G.; Freund, A. K. Nine-Crystal Multianalyzer Stage for High-Resolution Powder Diffraction between 6 and 40 keV. *Proc. SPIE* **1998**, *3448*, 353−361.
(20) Larson, A. C. and von Dreele, R. B. *General Structure Analysis System (GSAS)*; Los Alamos National Laboratory: Los Alamos, NM, 1994.
(21) Betteridge, P. W.; Carruthers, J. R.; Cooper, R. I.; Prout, K.; Watkin, D. J. CRYSTALS Version 12: Software for Guided Crystal Structure Analysis. *J. Appl. Crystallogr.* **2003**, *36*, 1487.
(22) Panella, B.; Hirscher, M.; Ludescher, B. Low-Temperature Thermal-Desorption Mass Spectroscopy Applied to Investigate the Hydrogen Adsorption on Porous Materials. *Microporous Mesoporous Mater.* **2007**, *103*, 230−234.
(23) Bauer, S.; Serre, C.; Devic, T.; Horcajada, P.; Marrot, J.; Férey, G.; Stock, N. High-Throughput Assisted Rationalization of the Formation of Metal Organic Frameworks in the Iron(III) Amino-terephthalate Solvothermal System. *Inorg. Chem.* **2008**, *47*, 7568−7576.
(24) Szilágyi, P. Á.; Lutz, M.; Gascon, J.; Juan-Alcañiz, J.; van Esch, J.; Kapteijn, F.; Geerlings, H.; Dam, B.; Van De Krol, R. MOF@MOF Core−Shell *vs.* Janus Particles and the Effect of Strain: Potential for Guest Sorption, Separation and Sequestration. *CrystEngComm* **2013**, *15*, 6003−6008.
(25) Lin, Y.; Kong, C.; Chen, L. Direct Synthesis of Amine-Functionalized MIL-101(Cr) Nanoparticles and Application for CO_2 Capture. *RSC Adv.* **2012**, *2*, 6417−6419.
(26) Botas, J. A.; Calleja, G.; Sánchez- Sánchez, M.; Orcajo, M. G. Cobalt Doping of the MOF-5 Framework and Its Effect on Gas-Adsorption Properties. *Langmuir* **2010**, *26*, 5300−5303.
(27) Hu, X.; Lu, Y.; Dai, F.; Liu, C.; Liu, Y. Host−Guest Synthesis and Encapsulation of Phosphotungstic Acid in MIL-101 *via* "Bottle around Ship": An Effective Catalyst for Oxidative Desulfurization. *Microporous Mesoporous Mater.* **2013**, *170*, 36−44.
(28) Turnes Palomino, G.; Palomino Cabello, C.; Otero Areán, C. Enthalpy−Entropy Correlation for Hydrogen Adsorption on MOFs: Variable-Temperature FTIR Study of Hydrogen Adsorption on MIL-100(Cr) and MIL-101(Cr). *Eur. J. Inorg. Chem.* **2011**, *11*, 1703−1708.
(29) Dybtsev, D.; Serre, C.; Schmitz, B.; Panella, B.; Hirscher, M.; Latroche, M.; Llewellyn, P. L.; Cordie, S.; Molard, Y.; Haouas, M.; et al. Influence of $[Mo_6Br_8F_6]^{2-}$ Cluster Unit Inclusion within the Mesoporous Solid MIL-101 on Hydrogen Storage Performance. *Langmuir* **2010**, *26*, 11283−11290.
(30) von Zeppelin, F.; Haluška, M.; Hirscher, M. Thermal Desorption Spectroscopy as a Quantitative Tool to Determine the Hydrogen Content in Solids. *Thermochim. Acta* **2003**, *404*, 251−258.